Supplementary Material for

Advection Influences the Firn Structure of Greenland's Percolation Zone

R. Leone, J. Harper, T. Meierbachtol, N. Humphrey

S1. Model Setup

S1.1 Firn Densification

We use the transient Herron and Langway (1980) (HL) model for firn densification, which is based on the assumption that the densification rate is linearly related to the change in overlying snow/ice load (Robin, 1958):

$$\frac{D\rho}{Dt} = \begin{cases} c_0(\rho_i - \rho) & \text{if} \quad \rho \leq \rho_c \\ c_1(\rho_i - \rho) & \text{if} \quad \rho_c < \rho \end{cases} \tag{S1}$$

where the critical density $\rho_c = 550$ kg m^{-3}. Temperature-dependent constants c_0 and c_1 are defined as:

$$\begin{cases} c_0 = 11\left(\frac{1000}{917}\right) b \cdot \exp\left(\frac{-10160}{RT}\right) & \text{if} \quad \rho \leq \rho_c \\ c_1 = 575\left(\frac{1000}{917}\right) b^{0.5} \cdot \exp\left(\frac{-21400}{RT}\right) & \text{if} \quad \rho_c < \rho \end{cases} \tag{S2}$$

where R is the gas constant (8.314 J K^{-1} mol^{-1}) and accumulation rate b is in ice equivalent units. We use an initial snow density (ρ_0) of 360 kg m^{-3} for the top boundary condition and an initial vertical velocity of $w = b \cdot \frac{\rho_w}{\rho_0}$. Equation S1 is then expanded out by applying the chain rule to the total derivate.

$$\frac{D\rho}{Dt} = \frac{\partial \rho}{\partial t} + w\frac{\partial \rho}{\partial z} \tag{S3}$$

S1.2 Temperature Evolution

Firn temperature was modeled by solving the standard one-dimensional time-dependent heat-transfer equation with latent heat from the refreezing of meltwater (Cuffey and Paterson, 2010).

$$\rho c \frac{\partial T}{\partial t} = k_T \frac{\partial^2 T}{\partial z^2} + \left[\frac{dk_T}{dz} - \rho c w\right]\frac{\partial T}{\partial z} + S \tag{S4}$$

where ρ is density, c heat capacity, k_T thermal conductivity, w vertical velocity, T temperature of the firn, and S as heat sources and sinks. We used thermal conductivity of firn as described in (Arthern and Wingham, 1998):

$$k_T = 2.1\left(\frac{\rho}{\rho_i}\right)^2 \tag{S5}$$

and a constant heat capacity for simplification. We use a constant boundary condition at the surface based on the annual mean air temperature.

S1.3 Horizontal Motion

In order to decrease run times and increase flexibility for including meltwater schemes, which are all 1D, we used a pragmatic approach that considers 1D model profiles moving through the percolation zone. Profiles are initiated high on the ice sheet and are transported through the percolation following a prescribed horizontal velocity, which is constant with depth. Horizontal motion through the percolation zone is achieved by translating spatially varying surface conditions (temperature and accumulation rate) to time-varying boundary conditions using surface velocities. This approach captures the processes of burial, ice layer formation/preservation, and vertical heat transport, but lacks horizontal heat diffusion.

S1.4 Firn Air Content

The capacity of the percolation zone to store meltwater is quantified by the firn air content. The cumulative air content is the integrated difference between infiltration ice density and firn density:

$$C(z) = \int_0^z \left(\rho_{ii}(\zeta) - \rho(\zeta)\right) d\zeta \tag{S6}$$

where ρ is firn density and ρ_{ii} is infiltration ice density, and z is depth. We used an average density of 843 kg m^{-3} for infiltration ice (Harper et al., 2012).

This calculation does not take into account perennial firn aquifers where capacity must be adjusted by 8.9% due to density differences between water and ice (Koenig et al., 2014). In order to obtain meters of air content of ice (and thus avoiding the complications that arise between the differences of water and ice density) we divide the total capacity by the density of ice.

S1.5 Horizontal Heat Transfer

To assess the consequences of neglecting horizontal heat diffusion in our modeling scheme, we developed an explicit 2D model for densification and heat transport for testing. While the formulation includes horizontal diffusion, it lacks meltwater infiltration schemes. In this formulation, 2D firn densification is defined as:

$$\frac{D\rho}{Dt} = \frac{\partial \rho}{\partial t} + w\frac{\partial \rho}{\partial z} + u\frac{\partial \rho}{\partial x} \tag{S7}$$

where *u* corresponds to the horizontal velocity. The temperature equation was also updated to include horizontal advection terms:

$$\rho c \frac{\partial T}{\partial t} = k_T \left(\frac{\partial^2 T}{\partial z^2} + \frac{\partial^2 T}{\partial x^2}\right) - \rho c u \frac{\partial T}{\partial x} + \left[\frac{dk_T}{dz} - \rho c w\right]\frac{\partial T}{\partial z} \tag{S8}$$

The surface boundary condition for temperature varied by several degrees across the surface domain to simulate the lower elevations of the percolation zone.

Both modeling frameworks were tested over a 90 km model domain, with a constant accumulation rate of 0.5 m a^{-1}. Surface temperature varied from -19 to -13 over the model domain, in approximate agreement with observations along the EGIG transect. Model simulations were executed with a prescribed surface velocity of 100 m a^{-1}, which approximates conditions along the EGIG transect, and with a surface velocity of 1000 m a^{-1} to test the consequences of neglecting horizontal diffusion under an extreme scenario.

Comparison results for the 100 m a^{-1} scenario are presented in Figure S1. The consequences of neglecting horizontal diffusion are negligible for both density and temperature results. Neglecting horizontal diffusion is more consequential when surface velocity is 1000 m a^{-1}, but even in this extreme scenario the maximum temperature difference is ~0.15°C; a difference which has essentially no impact on modeled density. This supports our modified approach, which we use for its flexible implementation of melt schemes and its fast runtime.

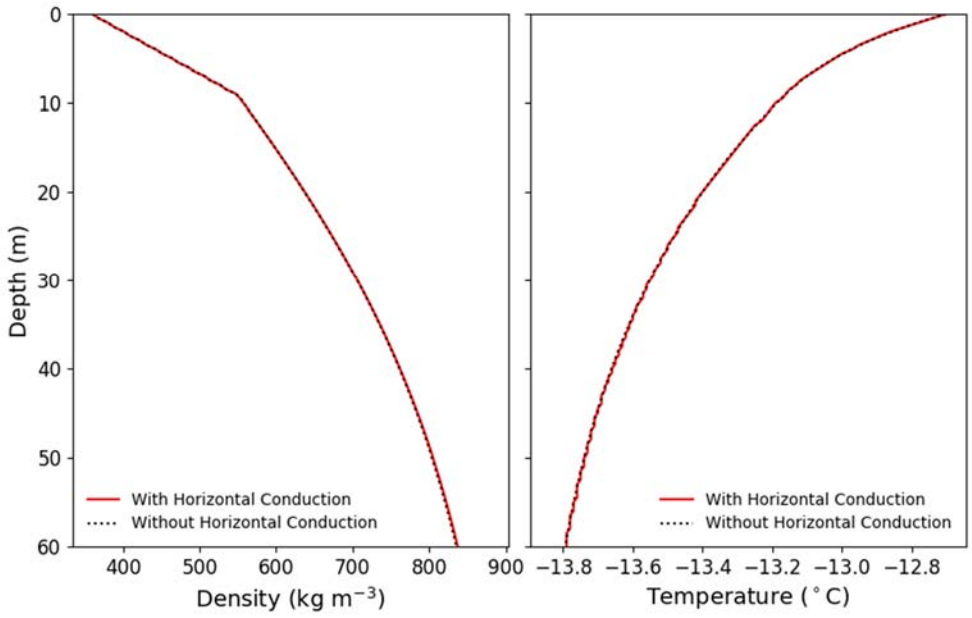

Figure S1. Simulated density (A) and temperature (B) results 80 km from the inland model boundary with, and without horizontal heat conduction.

S2.1 Sensitivity Testing

A range of sensitivity tests were performed to assess the role of ice forcing processes, in the presence of horizontal ice motion, on model results. Two dimensional simulations were performed over an 80 km model domain with constant velocity and accumulation. Surface temperature varied following a lapse rate and prescribed surface slope, and melt rates linearly increased along the model domain from zero at the model inland boundary, to a percentage of the accumulation value at the downstream boundary. This percentage was varied in testing. Two dimensional model results at 80 km were compared against 1D steady state results at that location. Sensitivity testing was performed around a base case scenario with horizontal velocity of 100 m a^{-1}, an

accumulation rate of 0.5 m a^{-1}, and melt rate of 85% of the accumulation at the lower model boundary.

Horizontal velocities were varied from 0 - 500 m a^{-1}, accumulation rates were varied from 0.1 - 1.0 m a^{-1} ice equivalent, and maximum melt was varied from 0 - 85% of the accumulation value. The ranges of values tested was chosen to approximately span the spectrum of conditions that may occur in GrIS' percolation zone. Additionally, we impose three different surface temperature gradients in each simulation to determine model sensitivity to a spatially varying surface temperature boundary. Simulations are performed for horizontal temperature gradients manifested in surface slopes of 0.3°, 0.6°, 0.8° assuming a temperature lapse rate of -7.4 °C/km (Fausto et al., 2009).

We used temperature at pore close off and total air content (see S1.2) as comparison metrics. Both 2D and 1D model simulations were performed for each sensitivity scenario, and the difference was calculated as a percentage:

$$\sigma_{\%diff} = \frac{\sigma_{2D} - \sigma_{1D}}{\left(\frac{\sigma_{1D} + \sigma_{2D}}{2}\right)} \quad \text{(S9)}$$

where σ is the metric of interest. Note that given this formulation, because firn temperatures are never >0°C, the denominator in S9 is negative and so temperatures in 2D simulations that are colder than the 1D counterpart reflect a positive difference.

S2.2 Sensitivity Test Results

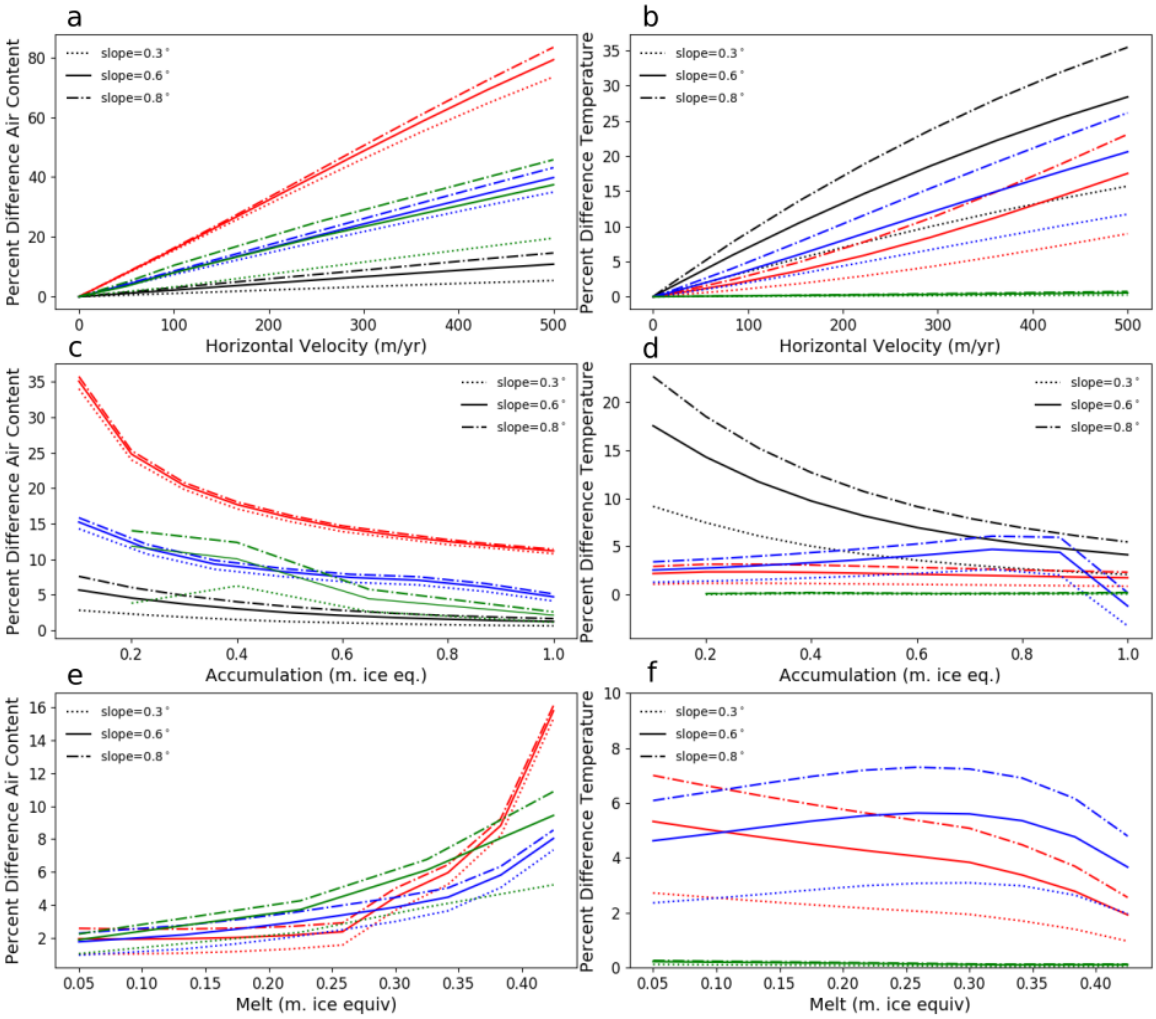

Figure S2. Modeled percent differences for sensitivity test forcings using dry model (black), Reeh model (red), tipping bucket model (blue), and continuum model (green). Left panels show percent difference in air content and right panels show percent differences in temperature. (a-b) show results from varying horizontal velocity, (c-d) represent testing of variable accumulation rates, and (e-f) show results for different melt rates.

S3. Model Results along GrIS Transects Under Different Melt Infiltration Schemes

The influence of horizontal ice flow on firn density and temperature is explored over 4 different GrIS transects. The difference between 2D and 1D model results is calculated as:

$$\sigma_{diff} = \sigma_{2D} - \sigma_{1D} \tag{S10}$$

where σ is the metric of interest. Figure S1 shows surface conditions; Figure S4 and S5 present results for the Reeh et al. (2005) and continuum meltwater infiltration schemes.

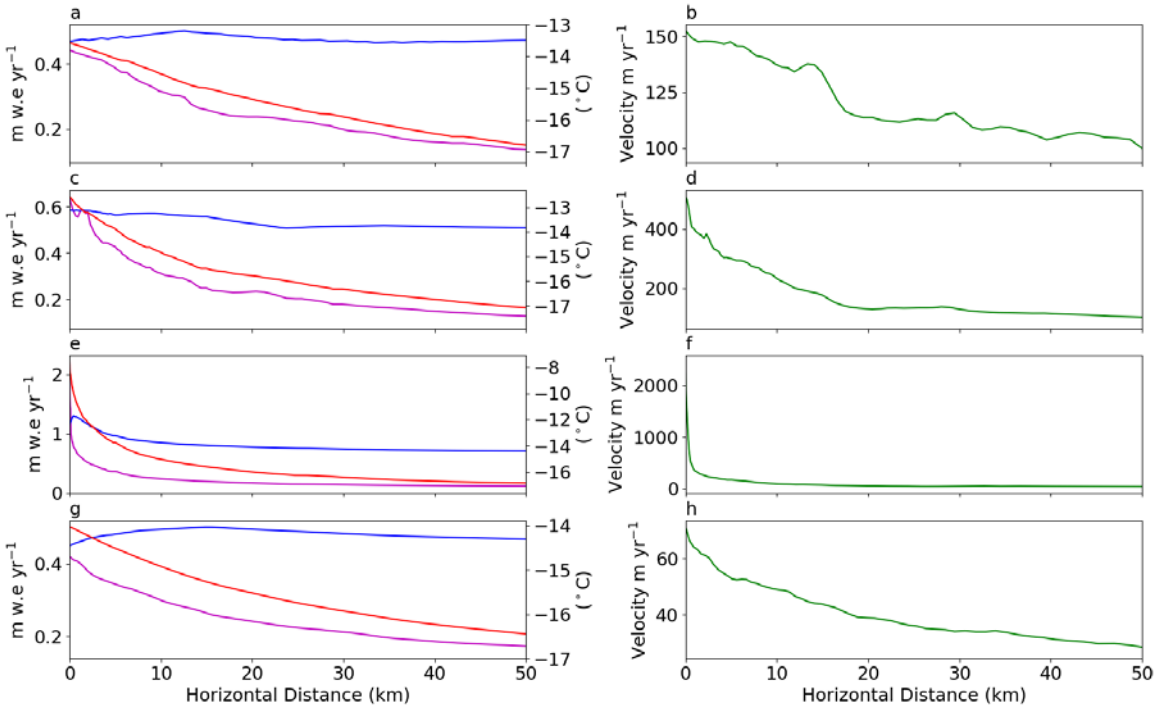

Figure S3. Surface conditions used for transect simulations. Left column shows snowfall (blue), temperature (red), and melt (magenta) extracted from RACMO2.3p2 (Noël et al., 2018) for 1980-2016 average. Right column snows speed extracted from (Joughin et al., 2010). Transects: EGIG (panels a,b); Jakobshavn (panels c,d); Helheim (panels, e,f); K-transect (panels g,h).

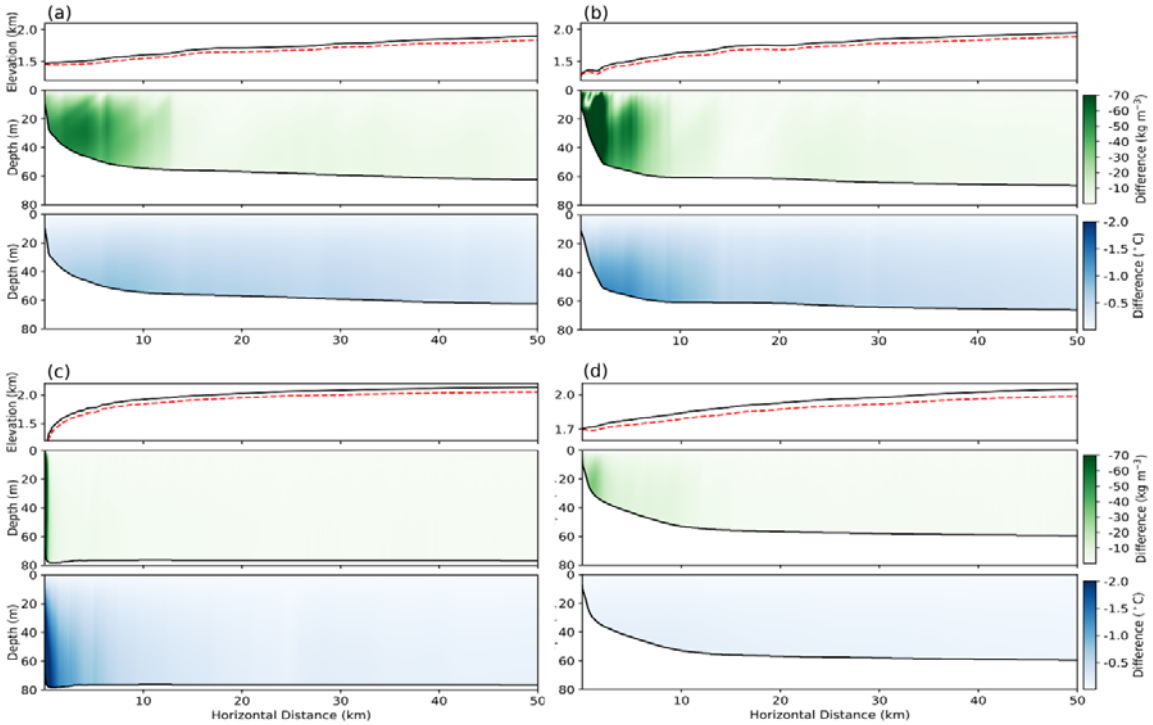

Figure S4. Modeled density and temperature differences between 1D and 2D results using the Reeh et al. (2005) infiltration scheme at the EGIG (a), Jakobshavn (b), Helheim (c), and K-transect (d). Top panel in each shows surface topography (black line) and 2D modeled depth to pore close-off (dashed red line).

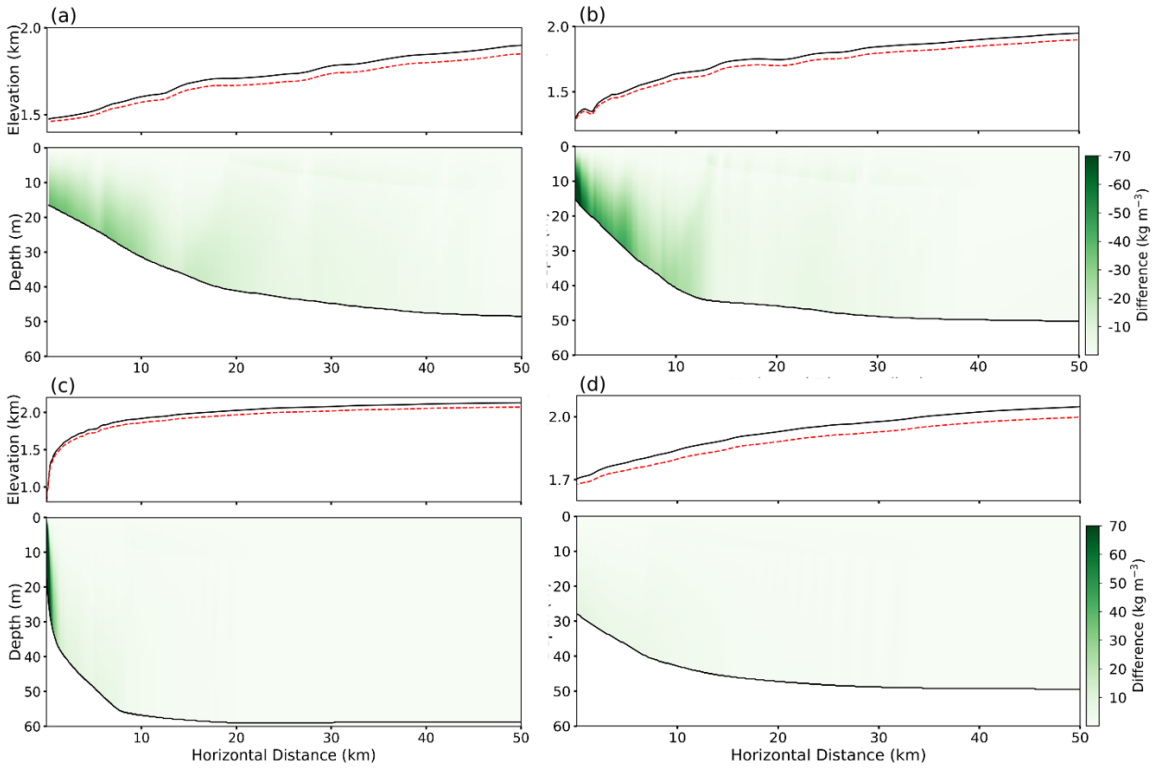

Figure S5. Modeled density differences between 2D and 1D simulations for GrIS transects as in Figure S3, but for the continuum meltwater infiltration scheme. Continuum model results were found to be insensitive to temperature (Figure S2) and are not displayed.

References

Arthern, R. J. and Wingham, D. J.: The natural fluctuations of firn densification and their effect on the geodetic determination of ice sheet mass balance, Clim. Change, 40(3–4), 605–624, 1998.

Cuffey, K. M. and Paterson, W. S. B.: The physics of glaciers, 4th Edition., 2010.

Fausto, R. S., Ahlstrøm, A. P., Van As, D., Johnsen, S. J., Langen, P. L. and Steffen, K.: Improving surface boundary conditions with focus on coupling snow densification

and meltwater retention in large-scale ice-sheet models of Greenland, J. Glaciol., 55(193), 869–878, doi:10.3189/002214309790152537, 2009.

Harper, J., Humphrey, N., Pfeffer, W. T., Brown, J. and Fettweis, X.: Greenland ice-sheet contribution to sea-level rise buffered by meltwater storage in firn, Nature, 491(7423), 240–243, doi:10.1038/nature11566, 2012.

Herron, M. M. and Langway, C. C.: Firn densification: an empirical model., J. Glaciol., 25(93), 373–385, doi:10.1017/S0022143000015239, 1980.

Joughin, I., Smith, B. E., Howat, I. M., Scambos, T. and Moon, T.: Greenland flow variability from ice-sheet-wide velocity mapping, J. Glaciol., 56(197), 415–430, doi:10.3189/002214310792447734, 2010.

Koenig, L. S., Miège, C., Forster, R. R. and Brucker, L.: Initial in situ measurements of perennial meltwater storage in the Greenland firn aquifer, Geophys. Res. Lett., 41(1), 81–85, doi:10.1002/2013GL058083, 2014.

Noël, B., Van De Berg, W. J., Van Wessem, J. M., Van Meijgaard, E., Van As, Di., Lenaerts, J. T. M., Lhermitte, S., Munneke, P. K., Smeets, C. J. P. P., Van Ulft, L. H., Van De Wal, R. S. W. and Van Den Broeke, M. R.: Modelling the climate and surface mass balance of polar ice sheets using RACMO2 - Part 1: Greenland (1958-2016), Cryosphere, 12(3), 811–831, doi:10.5194/tc-12-811-2018, 2018.

Reeh, N., Fisher, D. A., Koerner, R. M. and Clausen, H. B.: An empirical firn-densification model comprising ice lenses, in Annals of Glaciology, vol. 42, pp. 101–106., 2005.

Robin, G. de Q.: Glaciology III: Seismic Shooting and related investigations, Norsk Polarinstitutt., 1958.